Proceedings of the 17th World Congress
The International Federation of Automatic Control
Seoul, Korea, July 6-11, 2008

Hierarchical UAV Formation Control for Cooperative Surveillance ⋆

Andrew Sutton * **Barış Fidan*** **Dirk van der Walle** **

* *NICTA and the Australian National University, Canberra, ACT, Australia (e-mail: andrew.sutton@ieee.org, Baris.Fidan@anu.edu.au)*
** *Delft University of Technology, Delft, the Netherlands (e-mail: D.vanderWalle@student.tudelft.nl)*

Abstract: In this paper, we analyze the problem of rigidly maintaining a formation of three unmanned aerial vehicles (UAVs), whilst surveying a region of interest following, as a team, a particular pre-defined (spiral) trajectory. The UAVs in the formation are constrained to fly at constant speeds and to maintain certain pre-defined inter-agent distances. A decentralized proportional-integral (PI) control scheme (involving certain nonlinear switching terms) is developed for the surveillance and formation maintenance tasks above, based on a hierarchical (i.e. leader-first follower- second follower) sensing and control structure.

1. INTRODUCTION

A particular application area of multi-agent systems and cooperative control, which has been recently attracting growing interest, is cooperative localization and surveillance of targets Polycarpou et al. [2003], Marsh et al. [2007], Spletzer and Taylor [2003]. In this paper, we consider the task of co-operative scanning of a region of interest by a formation of 3 unmanned aerial vehicles (UAVs) *agent*s. For such a task, precise maintenance of a particular pre-defined formation, through close observation of inter-agent distances, is required for precision in locating targets. The task of autonomous formation maintenance requires the specification of a formation-wide control and sensing structure, in order to coordinate tasks among agents of the formation.

In formation control of autonomous multi-agent systems, one needs to consider and distinguish three different architectures: Sensing, control, and communication. Each of these architectures can be represented using a graph $G = (V, E)$ with a vertex set V and an edge set E, where each vertex $v_i \in V$ $(i \in 1, \ldots, |V|)$ represents an agent A_i, and each edge $e_{ij} \in E$ joining a certain pair of vertices $v_i, v_j \in V$ represents the (sensing, control, or communication) link between agents A_i and A_j. In this paper, a sensing link between agents A_i and A_j indicates that the inter-agent distance $|A_iA_j|$ is measurable by A_i and/or A_j, while a control link and a communication link between A_i and A_j indicate, respectively, that there is a constraint on the distance $|A_iA_j|$ to be satisfied by A_i and/or A_j and that A_i and A_j can communicate.

There are two main classes of the above architectures: Symmetric and asymmetric. In symmetric architectures, all the links are bidirectional, e.g. the distance constraint between any linked pair of agents (A_i, A_j) has to be satisfied by both A_i and A_j in a symmetric control architecture, while the links in asymmetric architectures are allowed to be unidirectional. Accordingly, the underlying (or representative) graphs $G = (V, E)$ of symmetric architectures are chosen to be undirected while asymmetric architectures are represented by directed underlying graphs. In this paper we consider an asymmetric control architecture, and using the above graph notation, a directed edge $\overrightarrow{(v_i, v_j)}$ from v_i to v_j indicates that agent A_i needs to maintain a pre-defined distance d_{ij} from agent A_j.

For asymmetric control architectures, the distributed control schemes can be classified in two groups based on the distribution of control tasks among agents: Hierarchical and non-hierarchical. In a hierarchical scheme, priority is placed over the information provided to agents. In this scheme control laws applied to an individual agent will depend upon the position and role of the agent within the formation. Details on hierarchical formation control schemes can be found in, e.g., Tanner et al. [2004], Anderson et al. [2006], Sandeep et al. [2006]. A non-hierarchical formation control scheme, on the other hand, applies identical priorities over all agents, where no leading agent is identifiable. Such schemes are explained and used in Anderson et al. [2006] and Anderson et al. [2007].

This paper focuses on the development of a hierarchical decentralized formation control scheme to be imposed upon a system of 3 UAV agents for robust performance and maintenance of an equilateral triangular formation whilst scanning a spiral path. The control scheme developed applies the principles of hierarchical control within a practical context of formation maintaining guidance for UAV surveillance.

2. COOPERATIVE SURVEILLANCE PROBLEM

2.1 The Overall Task

In this section, we give specifications of the particular task we focus on: cooperative surveillance over a 2-dimensional region of interest using a team of three UAVs. This task is part of a research challenge problem posed by the Australian Defence Science and Technology Organisation

⋆ NICTA is funded by the Australian Government as represented by the Department of Broadband, Communications and the Digital Economy and the Australian Research Council through the ICT Centre of Excellence program.

(DSTO) on localisation of targets with mobile sensors over large areas of interest Drake et al. [2005].

In this task, the three UAVs are equipped with bearing-only (or angle-of-arrival) measurement sensor units and are required to localize signal emitting targets, such as a radar station or similar. Due to the limitations on the sensing ranges of the UAVs, the scanning process is required to be accomplished by tracking of an spiral trajectory (with outward motion direction) originating at the center of a 2-dimensional region of interest R_S, which is specified to be a 30 km×30 km square in our case. In cartesian (x, y, z) coordinates, we assume that R_S lies on the $z = 0$ plane with center at $(x, y) = (0, 0)$. The other motivations behind the choice of the above spiral trajectory, as will be more apparent in Section 2.3, include its property of scanning the vicinity of the center (0,0) of R_S in a well-formulated polar form with constant increase rates of both the angle and radius and suitability for being tracked by an agent with a continuously decreasing turning rate. Note also that the results presented in this paper for this particular spiral path can be adapted to other smooth curves satisfying certain curvature constraints as well.

To obtain reliable results in such a bearing-only measurement based localization task, cooperation of at least three agents is necessary. Furthermore, the formation geometry of the UAV team is also important for accuracy of the localization results. These requirements dictate that a control scheme is required to maintain formation geometry. The optimal formation geometry for the bearing-only-measurement based surveillance task above is deduced, based on earlier relevant studies Bishop et al. [2007], Martinez and Bullo [2006], to be an equilateral triangle. The side length of the required equilateral triangular formation, in our case is, specified to be 3 km, based on the UAV specifications given in the sequel.

2.2 The UAV Agents and The Formation

The UAV model we use in this paper is based on the specifications of a specific UAV type named *Aerosonde* Ledger [2002], the type of the UAVs that are planned to be used in experimentation of a number of cooperative surveillance designs, including the one being studied here, by DSTO. *Aerosonde* is a small UAV, with a typical wing span of 2.9 m and a maximum take-off mass of 15 kg. It can fly continuously for 8–30 hours, depending on the payload it carries, without refuelling. The airspeed of the UAV is set to a constant value, between 20 m/s and 32 m/s, after take-off, and complying with the maximal airspeed of 32 m/s and minimum turning radius of 400 m, the maximum turning rate is $\omega_{max} = 0.08$ rad/s. In this paper, we assume that each of the three UAVs fly at a constant speed, and this constant speed is assumed to be the maximal speed 32 m/s, unless specified, noting we examine the effects of possible differences between the constant agent speeds later in the paper.

Each of the three UAVs is assumed to fly at a constant altitude (z-coordinate), parallel to R_S. Therefore we consider only the lateral (xy-coordinate) components of the UAV kinematics. Labelling the individual agents as A_1, A_2 and A_3, each agent A_i, $i \in \{1, 2, 3\}$ is assumed to move with the kinematics

$$\begin{aligned} \dot{x}_i(t) &= v_{ci} \cos\theta_i(t) \\ \dot{y}_i(t) &= v_{ci} \sin\theta_i(t) \\ \dot{\theta}_i(t) &= \omega_i(t) \end{aligned} \tag{1}$$

where $p_i(t) = (x_i(t), y_i(t)) \in \Re^2$ (xy-plane), $\theta_i(t)$ and $\omega_i(t)$ denote respectively the position, heading and angular velocity of A_i at time instant $t \geq 0$. For consistency, $\theta_i(t)$ shall be defined within the interval $(-\pi, \pi]$. It is also assumed that $\omega_i(t) \leq \omega_{max}, \forall t \geq 0 \quad (rad/sec)$.

As stated in Section 1, we use a hierarchical asymmetric control structure to maintain the equilateral triangular formation described Section 2.1. Using the notation in Section 1, we use a control architecture with the underlying graph $G = (V, E)$, $V = \{v_1, v_2, v_3\}$, $V = \{\overrightarrow{(v_2, v_1)}, \overrightarrow{(v_3, v_1)}, \overrightarrow{(v_3, v_2)}\}$, which is also illustrated in Fig. 1. There are two key notions useful in explaining the

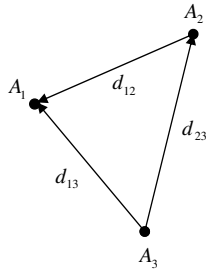

Fig. 1. The formation control architecture.

architecture selection above as well as being an essential basis for the symmetry and hierarchy classifications described in Section 1: *Rigidity* and *persistence*. Here we give the intuitive definitions of these two notions, leaving the formal definitions and further details to Hendrickx et al. [2007], Fidan et al. [2007] and the references therein: A *rigid formation* is one in which the only smooth motions are translations or rotations of the whole formation, i.e. a smoothly moving *rigid formation* maintains its geometry during motion once the nominated inter-agent distances are maintained. A rigid formation with asymmetric control structure is further called *persistent* if it is possible to maintain the nominated inter-agent distances.

It is worth to note that the control architecture depicted in Fig. 1, which is also named as the *leader-first follower-second follower structure* Fidan et al. [2007], Anderson et al. [2006], is the only hierarchical persistent one with three agents, where only single unidirectional links are allowed between agent pairs. In this architecture, A_1,A_2,A_3 are called, respectively, the *leader*, the *first follower (FF)*, and the *second follower (SF)* agents, since A_1 has no distance constraint to satisfy and will lead the formation via its motion, A_2 has single distance constraint to satisfy (with respect to A_1), and A_3 has two distance constraints to satisfy (with respect to both A_1 and A_2).

The leader agent A_1 is responsible for the tracking of the desired trajectory, which is described in the next section. Agent A_2 is required to (i) track A_1 at the desired distance (with certain error tolerance) $d_{12} \pm \epsilon_{12}$ (d_{12}=3 km, ϵ_{12}=5 m) and (ii) align its heading direction with that of A_1, with no knowledge of the intended trajectory. Finally, Agent A_3 is required to track both A_1 and A_2, at desired separation distances with certain

error tolerances) $d_{13} \pm \epsilon_{13}$ and $d_{23} \pm \epsilon_{23}$, respectively ($d_{13} = d_{23}$=3 km, $\epsilon_{13} = \epsilon_{23}$=15 m).

Each agent A_i is assumed to sense the location $p_i(t)$ of itself as well as the position of the agent(s) it has to follow, for all t. Furthermore A_1 is assumed to know the spiral path to be tracked by the formation, which is explained in detail in the following subsection. There shall be no co-operation, other than that dictated by the control structure, or other forms of communication allowed between agents.

2.3 Spiral Path and Way-Points

The surveillance path is taken as an Archimedean spiral originating from a point close to the center (0,0) of R_S. This spiral path can be formulated in time-indexed form in 2-dimensional polar coordinates $(r, \bar{\theta})$ corresponding to the cartesian coordinates $(x, y) = (r\cos\bar{\theta}, r\sin\bar{\theta})$, with the starting point at $(\alpha, 0)$ (in both polar and cartesian coordinates), as

$$r(t) = \alpha + \beta\bar{\vartheta}(t) \qquad (2)$$
$$\bar{\theta}(t) = \bar{\vartheta}(t) \pmod{2\pi}$$

where $\bar{\vartheta}(t)$ is a monotonically increasing function of t satisfying $\bar{\vartheta}(0) = 0$ and $\lim_{t\to\infty} \bar{\vartheta}(t) = \infty$, and the design constants $\alpha, \beta \geq 0$ denote, respectively, the initial radial offset and the radial increase per revolution.

As also stated in Section 2.2, Agent A_1 is responsible to survey over the surveillance, the spiral path formulated in (2). Sampling this spiral path at regular intervals permits the generation of a *way-point* trajectory for A_1 to follow, which can be expressed as a set W of m cartesian way-points over the trajectory:

$$W = \{w_n\}_{n=0}^{n=\bar{n}} \qquad (3)$$

where $w_0 = (\alpha, 0)$, and the order of way-points obeys the time-ordering of their representation in (2), i.e. if for each $0 \leq n \leq \bar{n}$ the polar coordinates of w_n are denoted by $(r_{wn}, \bar{\theta}_{wn})$ and $r_{wn} = \alpha + \beta\bar{\vartheta}(t_n)$, then $t_n < t_{n+1}$ for any $0 \leq n < \bar{n}$. Furthermore, in order to guarantee that the formation follows (2) within acceptable turning radius tolerances, it successive way-points are selected such that they satisfy $\|w_n - w_{n+1}\| \leq 500$ m.

2.4 Control Problem Definition

The cooperative surveillance task introduced in Section 1 and detailed in Sections 2.1–2.3 is formally summarized in the following problem definition. Note that this problem definition is rather from the practical control design perspective than describing the ideal desired motion of the 3-UAV formation, and is stated in terms of the way-points (3) instead of the ideal desired spiral path (2).

Problem 1. Consider three UAV agents A_1,A_2,A_3 moving with agent kinematics (1) and the control architecture in Fig. 1. Let us be given the way-points defined by (3) and a small pre-defined way-point precision constant $\epsilon_w > 0$, and let $\mathcal{B}_{wk}$ $(0 \leq k \leq \bar{n})$ denote the closed ball with center w_k and radius ϵ_w. Generate the control signals $\omega_i(t)$, $\forall t \geq 0$ $(i \in \{1, 2, 3\})$ such that
(i) $|\|p_i(t) - p_j(t)\| - d_{ij}|$, where $d_{ij} = 3$ km, is minimized, with the ultimate goal of satisfying $|\|p_i(t) - p_j(t)\| - d_{ij}| \leq \epsilon_{ij}$, for any $i, j \in \{1, 2, 3\}$, $i \neq j$ and any time $t \geq 0$.
(ii) $\|p_1(t) - w_{n_1(t)+1}\|$ is minimized for any time $t \geq 0$ before A_1 reaches $\mathcal{B}_{w\bar{n}}$, where $n_1(t) \in \{0, 1, \ldots, \bar{n}\}$ denotes the largest index $n \in \{0, 1, \ldots, \bar{n}\}$ for which $\mathcal{B}_{wn}$ is visited by A_1 at or before t.

3. HIERARCHICAL FORMATION CONTROL DESIGN

In this section we develop a set of individual control laws to be used by the UAVs within the hierarchical formation control framework described in Sections 1 and 2. Each of the individual controllers is to be developed under a common framework described by the generic system block diagram shown in Fig. 2. We assume that the individual agents have been controlled to within a small tolerance of their initial starting positions by another control scheme.

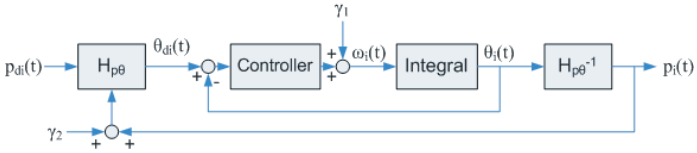

Fig. 2. Control system of agent A_i $(i \in \{1, 2, 3\})$.

In this framework, the input of the individual control system of A_i $(i \in \{1, 2, 3\})$ is the desired position $p_{d_i}(t)$ of A_i at time t, the selection of which is discussed later. The output $p_i(t)$ is the actual position of the agent within $R_S \subset \Re^2$ at time t, as a result of the control signal $\dot{\theta}_i = \omega_i$. The function $H_{p\theta}$ represents the non-linear mapping of the desired motion direction vector $p_{d_i}(t) - p_i(t)$ into a scalar *desired heading* $\theta_{d_i}(t)$.

The purpose of the internal feedback loop is to drive the agent orientation $\theta_i(t)$ to the desired heading $\theta_{d_i}(t)$. $H_{\theta p}$ represents the generation of the position $p_i(t)$ from the heading $\theta_i(t)$ according to (1). γ_1 and γ_2 represent the cumulative effects of the actuator and (position) sensor noises, respectively.

For each agent A_i $(i \in \{1, 2, 3\})$, irrespective of being a leader, a first follower, or a second follower agent, we propose the proportional integral (PI) feedback control law

$$\omega_i(t) = k_{i1}[\theta_{d_i}(t) - \theta_i(t)] + k_{i2}\int_{t_0}^{t}[\theta_{d_i}(t) - \theta_i(t)]dt \qquad (4)$$

where $k_{i1}, k_{i2} > 0$ are the design coefficients for the proportional and integral gains.

The generation of the desired agent heading $\theta_{d_i}(t)$, which is used as the reference signal in (4), differs for each A_i and is explained in detail in the following subsections.

3.1 Leader Agent Controller

Based on the agent specifications of in Section 2.2, the individual task of the controller of the leader agent A_1 within Problem 1 is as follows: Generate the control signal $\omega_1(t)$, $\forall t \geq 0$ such that $\|p_1(t) - w_{n_1(t)+1}\|$ is minimized for any time $t \geq 0$ before A_1 reaches $\mathcal{B}_{w\bar{n}}$.

In order to meet this task, the desired agent heading $\theta_{d_1}(t)$ (to be used in the control law (4) for $i = 1$) is defined as the heading from the agent's *current position* $p_1(t)$ to the *target position* $p_{d_1}(t) = w_{n_1(t)+1}$, i.e.

$$\theta_{d_1}(t) = \angle(w_{n_1(t)+1} - p_1(t)) \qquad (5)$$

3.2 First Follower Agent Controller

Again based on the agent specifications of in Section 2.2, the individual task of the controller of the first follower agent A_2 within Problem 1, any time $t \geq 0$, is generating the control signal $\omega_2(t)$ such that
(i) $|\|p_1(t) - p_2(t)\| - d_{12}|$, where $d_{12} = 3$ km, is minimized, with the ultimate goal of satisfying $|\|p_1(t) - p_2(t)\| - d_{12}| \leq \epsilon_{12}$.
(ii) $\|\theta_1(t) - \theta_2(t)\|$ is minimized.

Note that in generation of $\omega_2(t)$, the criterion (ii) is considered only at the time instants t for which $|\|p_1(t) - p_2(t)\| - d_{12}| \leq \epsilon_{12}$. In order to determine a generation law for $\omega_2(t)$, we consider the following three cases depending on the value of the distance keeping error $e_{12}(t) \triangleq \|p_1(t) - p_2(t)\| - d_{12}$:

Case 1 : $e_{12}(t) < -\epsilon_{12}$**.** The distance between A_1 and A_2 is smaller than required. A_2 needs to be headed away from A_1. Hence, its desired heading is assigned as $\theta_{d_2}(t) = \angle(p_{1(t)} - p_2(t)) + \pi$.

Case 2: $e_{12}(t) > \epsilon_{12}$**.** The distance between A_1 and A_2 is larger than required. A_2 needs to be headed towards A_1. Hence, its desired heading is assigned as $\theta_{d_2}(t) = \angle(p_{1(t)} - p_2(t))$.

Case 3: $-\epsilon_{12} \leq e_{12}(t) \leq \epsilon_{12}$**.** A_1 is correctly maintaining the desired separation distance to within a specified tolerance of magnitude ϵ_{12}. A_2's task in this case is to estimate and converge to the heading $\theta_1(t)$ of A_1. The estimate $\hat{\theta}_1(t)$ is obtained applying linear interpolation on the previous position information of A_1:

$$\hat{\theta}_1(t) = \angle(p_1(t) - p_1(t - T_\Delta))$$

where T_Δ is the interpolation delay term (taken as 0.1 sec in this work).

Based on the discussions of the three cases above, the desired agent heading, to be used in conjunction with the PI-controller (4), for agent A_2 is generated as follows:

$$\theta_{d_2}(t) = \begin{cases} \angle(p_{1(t)} - p_2(t)) + \pi & , \text{ if } e_{12}(t) < -\epsilon_{12} \\ \angle(p_{1(t)} - p_2(t)) & , \text{ if } e_{12}(t) > \epsilon_{12} \\ \hat{\theta}_1(t) & , \text{ if } -\epsilon_{12} \leq e_{12}(t) \leq \epsilon_{12} \end{cases}$$

3.3 Second Follower Agent Controller

Similarly to the agents A_1 and A_2, the individual task of the controller of the second follower agent A_3 within Problem 1, at any time $t \geq 0$, is generating the control signal $\omega_2(t)$ such that $|\|p_i(t) - p_3(t)\| - d_{i3}|$, where $d_{i2} = 3$ km, is minimized for $i \in \{1, 2\}$, with the ultimate goal of satisfying $|\|p_i(t) - p_3(t)\| - d_{i3}| \leq \epsilon_{i3}$.

Similarly to the first follower agent controller in Section 3.2, the desired heading $\theta_{d_3}(t)$ shall be selected considering two cases depending on the values of $e_{i3}(t) \triangleq \|p_i(t) - p_3(t)\| - d_{i3}$ for $i \in \{1, 2\}$:

Case 1: $|e_{13}(t)| > \epsilon_{13}$ **or** $|e_{23}(t)| > \epsilon_{23}$**.** At least one of the two distance constraints for A_3 is not satisfied within the separation tolerance. A_3 is headed to the closest intersection point $\bar{p}_{12}(t, p_3(t))$ of the circles of radius $d_3 > 0$ centered at $p_1(t)$ and $p_2(t)$, which are denoted, similarly to Sandeep et al. [2006], by $C(p_1(t), d_{13})$ and $C(p_2(t), d_{23})$, respectively.

Case 2: $|e_{13}(t)| \leq \epsilon_{13}$ **and** $|e_{23}(t)| \leq \epsilon_{23}$**.** Both of the two distance constraints for A_3 are satisfied within the separation tolerance. A_3's task in this case is to estimate the motion direction $\hat{\theta}_{\bar{p}_{12}}(t)$ of $\bar{p}_{12}(t, p_3(t))$ and move in this direction. The estimate $\hat{\theta}_{\bar{p}_{12}}(t)$ is obtained applying linear interpolation on the previous position information of $\bar{p}_{12}$:

$$\hat{\theta}_{\bar{p}_{12}}(t) = \angle(\bar{p}_{12}(t, p_3(t)) - \bar{p}_{12}(t - T_\Delta, p_3(t - T_\Delta)))$$

where $T_\Delta = 0.1sec$ as defined in Section 3.2.

Note here that in Case 1, in order to have a valid definition for all situations including the cases where $C(p_1(t), d_{13})$ and $C(p_2(t), d_{23})$ do not intersect (which are unexpected when there is no noise or disturbances affecting the agent systems illustrated in Fig. 2 and rarely expected when there is noise/disturbance), we formally define $\bar{p}_{12}(t, p_3(t))$ as follows:

$$\bar{p}_{12}(t, p_3(t)) = \begin{cases} \arg\min\{\|p - p_i\| \mid p \in C(p_1(t), d_{13}) \cap \\ \quad C(p_2(t), d_{23})\} \text{ if } \|p_1(t) - p_2(t)\| \leq d_{12} + d_{13} \\ \frac{1}{2}(p_1(t) + p_2(t)) \quad \text{else} \end{cases} \tag{6}$$

Based on the discussions above, the desired agent heading, to be used as the reference signal of the PI-controller (4), for agent A_3 is generated as follows:

$$\theta_{d_3}(t) = \begin{cases} \angle(\bar{p}_{12}(t, p_3(t)) - p_3(t)) & , \text{ if } |e_{13}(t)| > \epsilon_{13} \\ & \quad \text{or } |e_{23}(t)| > \epsilon_{23} \\ \hat{\theta}_{\bar{p}_{12}}(t) & , \text{ else} \end{cases}$$

4. SIMULATIONS AND NUMERICAL ANALYSIS

In this section, we analyze characteristics of the decentralized control scheme developed in Section 3 and its performance in meeting the requirements of Problem 1.

We use the system parameter values given in Section 2. The values not specified in Sections 2,3 are selected as follows: In (2), the spiral parameters are selected as $\alpha = 0, \beta = \frac{9000}{2\pi} m$. The respective controller gains in (4) are selected as follows: $k_{11} = k_{21} = 4$, $k_{12} = k_{22} = 0.0005$, $k_{31} = 1$, $k_{32} = 0.5$. Agents A_1 and A_2 have identical control gains, which have been tuned for the desired performance. The Second Follower integral gain is increased to reduce high frequency chatter effects.

4.1 Noise-Free Case

In the absence of any noise or disturbance, the resulting system performance is presented in Fig. 3 (a) and (b). The trajectory paths in (a) show that the desired spiral trajectory has been tracked successfully with error specified in (b). Noting that the desired separation is $d_{ij} = 3$ km for any agent pair A_i,A_j and the allowed tolerances are $\epsilon_{12} = 5$m, $\epsilon_{13} = \epsilon_{23} = 15$m, it is clear from the plots that the distance keeping tasks are performed successfully and the tolerances were attained after start-up transients had decayed. These transients primarily result from the non-ideal initialization of agent headings and position. The chatter effects evident in the second follower position error could be minimized by a carefully selected smoothing filter for the heading control.

4.2 Noise And Disturbance Effects

To ensure robust system performance, the developed hierarchical decentralized control scheme has been simulated under two distinct types of noise; global positioning noises (represented by γ_2 in Fig. 2) and UAV air-speed offsets. The positioning noise γ_2 represents the inaccuracies in the

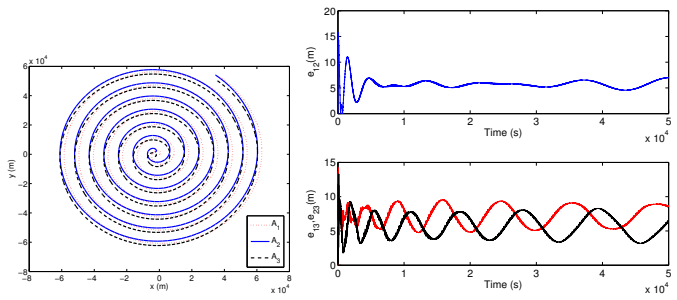

(a) (b)

Fig. 3. Typical surveillance behavior over 50,000 sec: (a) Formation trajectory. (b) Inter-agent separation errors e_{ij} noting that $d_{12} = d_{13} = d_{23} = 3000$ m.

inter-agent separation distance measurements. The UAV air-speed offsets are constant differences of the individual UAVs from the maximal (nominal) value 32 m/s indicated in Section 2, and are in general different for different agents.

4.3 Positioning Error

Positioning error relates to the inherent uncertainty introduced when agent positioning determined by any form of measurement, such as GPS systems or laser range finding. Depending upon measurement quality, the position accuracy of an agent can be determined to within less than a meter in good conditions and out to several hundred meters in exceptionally poor situations. Since the control methods developed rely heavily upon measurement of inter-agent separation distances, the effects of this form of error upon the system need to be analyzed.

In our simulations, the positioning error in each agent is modelled (identically among the agents) by an additive Gaussian noise with zero mean and variance σ^2. The simulation mean-square-error results have been calculated for a range of noise variances from $\sigma^2 = 0$ to $150m^2$ and the results are plotted in Fig. 4.

Fig. 4 (a) indicates that A_2 performs acceptably in the presence of sensor noise, as the MSE is maintained below the 5m tolerance specified for e_{12}. The error surfaces shown in Fig. (b) and (c) show that A_3 performance degrades gracefully as the noise variance increases. The system also remains stable under all conditions tested. This result is highly desirable, as it indicates that the system is robust against sensor noise sources, however performance is compromised.

In particular, by comparing the error magnitudes for A_2 and A_3 shown in Fig. 4, it is evident that A_3 is most severely affected by sensor noise. The distance constraint placed upon A_3 by A_2 dictates that the sensor noise power applied to A_2 dominates the performance of A_3. This is shown in the error plots in Fig. (b) and (c), where the error surface is dominated by A_2 noise variance, with a weak dependence upon A_3 noise.

The most severe case tested corresponds to a noise of $\sigma^2 = 150m^2$ applied to all agents. The trajectories traced by the agents under this noise magnitude are shown in Fig. 4 (d), which demonstrates that there is no immediately visible affects of sensor noise upon tracking. However, the MSE error plots, with $\sigma^2 = 150m^2$, show that the average

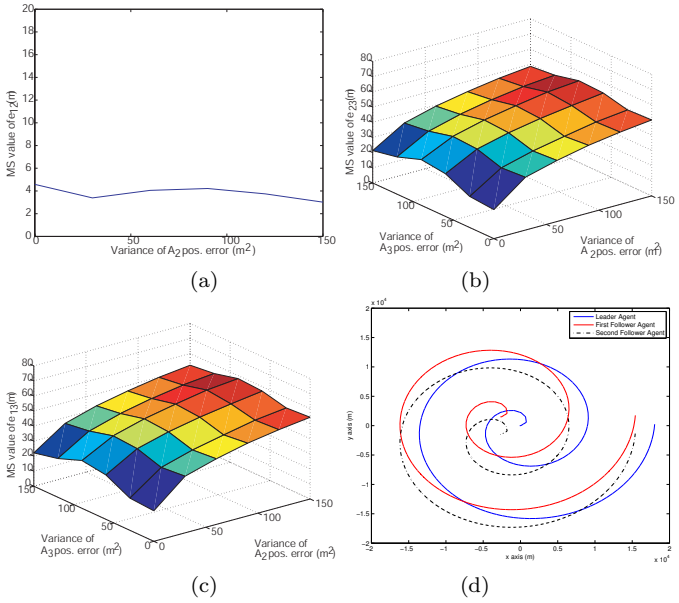

(a) (b) (c) (d)

Fig. 4. A 4000 sec simulation with position error variances $\sigma^2 = 0m^2 - -150m^2$: (a) Mean-square distance keeping error (MSE) between A_1–A_2. (b) MSE between A_2–A_3. (c) MSE between A_1–A_3. (d) The trajectory tracked for $\sigma^2 = 150m^2$ over a 4 km × 4 km area.

MSE for the inter-agent separation distances is growing with increased noise variance.

4.4 Air Speed Offsets

A common situation occurring amongst individual UAVs in is variability of the air speeds. Between any two agents, it is expected that the cruising air speed may differ by up to 10°% of the nominal air speed. The UAV specifications from Section 2.2 do not allow any active control of agent speeds. However one can still consider the values of the different individual speeds in selection of the specific agent for assigning each of the leader, first-follower and second-follower roles within the hierarchical control structure described in Section 2.2: The slowest agent within the formation needs to take the leader agent role, as it can be easily observed that, otherwise, at least one agent would not be able to maintain its constant distance requirements always. With a similar reasoning, the speed of the first follower agent needs to be slower than or equal to the second follower. Nevertheless, the effects of various selections, including even some with first follower faster than the second follower, can be seen in the simulation results presented in the sequel.

Fig. 5 shows the results of a series of simulations performed to determine the effects of varying the first follower and the second follower agent air speeds by up to 10%, compared to the leader agent, where, considering the speed variation effects, all the three interagent distance keeping error tolerances are increased to $\epsilon_{ij} = 30$ m/s. The most notable feature of the Fig. 5 (a) is bound on the MS error at around 30 m, which is the error tolerance specified for this simulation. The situation is considerably different for Fig. 5(b) and 5(c). For situations where $v_{c3} > v_{c2}$, the error surface is relatively smooth, however the magnitude of this error is still significantly larger than $\epsilon_{ij} = 30$ m. In contrast, when $v_{c3} < v_{c2}$, the MS error grows significantly

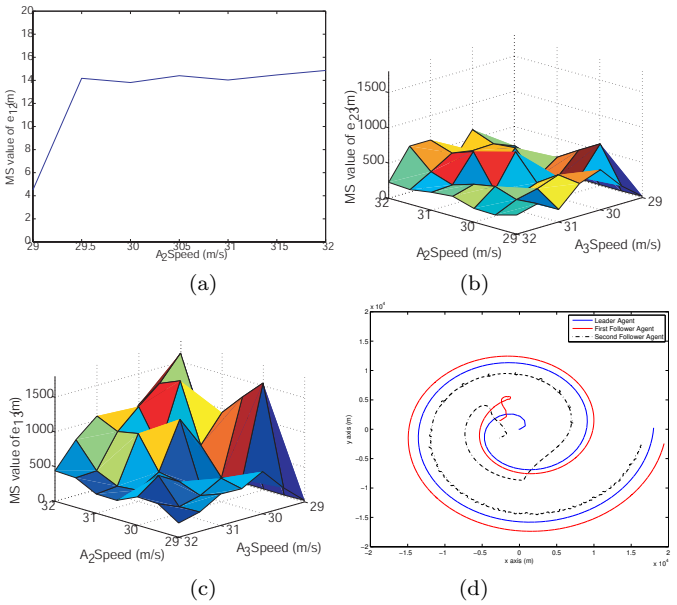

Fig. 5. A 4000 sec simulation with agent speeds $v_{c1} = 29$ m/s and v_{c2}, v_{c3} constants between 29–32 m/s: (a) Mean-square distance keeping error (MSE) between A_1–A_2. (b) MSE between A_2–A_3. (c) MSE between A_1–A_3. (d) The trajectory tracked for $v_{c1} = 29$ m/s , $v_{c2} = v_{c3} = 32$ m/s over a 4 km $\times$ 4 km area.

and A_3 is unable to quickly track A_2, which is circling around A_1 with its excess speed.

Fig. 5(d) shows a particular scenario where $v_{c2} = v_{c3} = 32$ m/s and $v_{c1} = 29$ m/s. In this case, the most obvious cause of error in the system is the 'loops' performed by A_3 as it tries to meet its distance constraints. A potential solution for the problems caused by air speed differences between agents is to introduce sinusoidal heading oscillation, with magnitude proportional to the speed differences.

5. CONCLUSION

In this paper, we have developed a hierarchical decentralized control scheme for a formation of 3 surveillance UAV agents tracking a spiral trajectory. The control scheme is composed of a leader-first follower-second follower control structure and an individual PI-controller with desired heading as a reference signal for each agent. The desired heading signals have different nature for different agents depending on their individual task within the hierarchical control structure. The performance designed control scheme and its robustness to position sensor noises and agent speed offsets is successfully tested via a series of simulations. The simulation results indicate that the UAV formation meets its control tasks even in the case of mild sensor noises and air-speed offsets. Nevertheless, increase in these noises and offsets affect the system performance significantly. Potential future work includes compensation of these affects. For compensation of the sensor and actuator noises, the potential direction is introduction of robust and/or adaptive control techniques depending on the a priori information available. For compensation of the individual agent speed offsets, a particular research task, which is currently being pursued by the authors, is introduction of sinusoidal heading oscillations in a systematic way where the magnitude and frequency of the sinusoidal component would be determined by the air-speed offset from the nominal value and the kinematic (e.g. turning rate) constraints on the UAV agents. A more general future research task is more formal analysis of the system stability, performance, and robustness.

REFERENCES

B. D. O. Anderson, C. Yu, S. Dasgupta, and A. S. Morse. Control of a three coleaders formation in the plane. *Systems and Control Letters*, 56:573–578, 2007.

B. D. O. Anderson, C. Yu, B. Fidan, and J. M. Hendrickx. Control and information architectures for formations. In *Proc. IEEE International Conf. on Control Applications*, pages 1127–1138, Munich, Germany, October 2006.

A.N. Bishop, B. Fidan, B.D.O. Anderson, K. Dogancay, and P.N. Pathirana. Optimality analysis of sensor-target geometries in passive localization: Part 1 - bearing-only localization. In *Proc. 3rd Int. Conf. on Intelligent Sensors, Sensor Networks and Information Processing (ISSNIP)*, pages 7–12, Melbourne, VIC, Australia, December 2007.

S. Drake, K. Brown, J. Fazackerley, and A. Finn. Autonomous control of multiple UAVs for the passive location of radars. *Proc. Int. Conf. on Intelligent Sensors, Sensor Networks and Information Processing (ISSNIP)*, pages 403–409, December 2005.

B. Fidan, B. D. O. Anderson, C. Yu, and J. M. Hendrickx. *Modeling and Control of Complex Systems*, chapter Persistent Autonomous Formations and Cohesive Motion Control. Taylor & Francis, 2007.

J. M. Hendrickx, B. D. O. Anderson, J.-C. Delvenne, and V. D. Blondel. Directed graphs for the analysis of rigidity and persistence in autonomous agent systems. *International Journal of Robust and Nonlinear Control*, 17:960–981, July 2007.

D. Ledger. Electronic warfare capabilities of mini UAVs. In *Proc. the Electronic Warfare Conference*, Kuala Lumpur, 2002.

L. Marsh, D. Gossink, S. P. Drake, and G. Calbert. UAV team formation for emitter geolocation. *IEEE Conference on Decision and Contol*, pages 176–181, February 2007.

S. Martinez and F. Bullo. Optimal sensor placement and motion coordination for target tracking. *Automatica*, 42 (3):661–668, March 2006.

M. Polycarpou, Y. Yang, Y. Liu, and K. Passino. *Cooperative Control: Models, Applications and Algorithms*, chapter Cooperative Control Design for Uninhabited Air Vehicles, pages 283–321. Kluwer Academic Publishers, 2003.

S. Sandeep, B. Fidan, and C. Yu. Decentralized cohesive motion control of multi-agent formations. *Proc. 14th Mediterranean Conference on Control and Automation*, June 2006.

J. R. Spletzer and C. J. Taylor. Dynamic sensor planning and control for optimally tracking targets. *The International Journal of Robotics Research*, 22(1):7–20, 2003.

H. G. Tanner, G. J. Pappas, and V. Kumar. Leader-to-formation stability. *IEEE Trans. on Robotics and Automation*, 20(3):443–455, June 2004.